Theor Ecol (2014) 7:163–179
DOI 10.1007/s12080-013-0208-2

ORIGINAL PAPER

Infectious disease in consumer populations: dynamic consequences of resource-mediated transmission and infectiousness

Paul J. Hurtado · Spencer R. Hall · Stephen P. Ellner

Received: 27 June 2013 / Accepted: 14 November 2013 / Published online: 17 January 2014

Abstract Nonhost species can strongly affect the timing and progression of epidemics. One central interaction—between hosts, their resources, and parasites—remains surprisingly underdeveloped from a theoretical perspective. Furthermore, key epidemiological traits that govern disease spread are known to depend on resource density. We tackle both issues here using models that fuse consumer–resource and epidemiological theory. Motivated by recent studies of a phytoplankton–zooplankton–fungus system, we derive and analyze a family of dynamic models for parasite spread among consumers in which transmission depends on consumer (host) and resource densities. These models yield four key insights. First, host–resource cycling can lower mean host density and inhibit parasite invasion. Second, host–resource cycling can create Allee effects (bistability) if parasites increase mean host density by reducing the amplitude of host–resource cycles. Third, parasites can stabilize host–resource cycles; however, host–resource cycling can also cause disease cycling. Fourth, resource dependence of epidemiological traits helps to govern the relative dominance of these different behaviors. However, these resource dependencies largely have quantitative rather than qualitative effects on these three-species dynamics. Given the extent of these results, host–resource–parasite interactions should become more fundamental components of the burgeoning theory for the community ecology of infectious diseases.

Keywords Host–parasite · Predator–prey · Transmission rate · Oscillations · Hydra effect · *Daphnia*

Electronic supplementary material The online version of this article (doi:10.1007/s12080-013-0208-2) contains supplementary material, which is available to authorized users.

P. J. Hurtado (✉)
Center for Applied Mathematics, Cornell University,
Ithaca, NY 14853, USA
e-mail: hurtado.10@mbi.osu.edu

S. R. Hall
Department of Biology, Indiana University,
Bloomington, IN 47405, USA

S. P. Ellner
Center for Applied Mathematics, Department of Ecology and Evolutionary Biology, Cornell University,
Ithaca, NY 14853, USA

Present Address:
P. J. Hurtado
Mathematical Biosciences Institute, The Ohio State University,
Columbus, OH 43221, USA

Introduction

Disease ecology has traditionally focused on the epidemiological and coevolutionary relationships between hosts and their parasites. This approach has produced powerful insights into the drivers of infectious disease epidemics. Recently, however, theoretical and empirical research have increasingly supported the idea that other species can modulate the spread of infectious disease (e.g., Keesing et al. 2006; Hatcher et al. 2006). As a result, several sets of core interactions between host, parasite, and other species have garnered deserved attention. For instance, predators that selectively prey on infected hosts can depress disease prevalence (Packer et al. 2003; Ostfeld and Holt 2004; Hall et al. 2005), although other predators can also facilitate the spread of disease (Holt and Roy 2007; Cáceres et al. 2009; Duffy et al. 2011). Additionally, incompetent host species may

inhibit disease through a "dilution effect" (Norman et al. 1999; Ostfeld and Keesing 2000; Holt et al. 2003; Keesing et al. 2006; Hall et al. 2009b). These examples illustrate the importance of building theory for the community ecology of infectious diseases.

One interaction currently warrants much more development. While potentially being parasitized, hosts also consume resources. In fact, many hosts strongly interact with and depress the abundance of their resources (e.g., *Daphnia* consume algae; gypsy moths can defoliate forests: Ebert 2005; Dwyer et al. 2004). It seems possible that inherent properties of the host–resource interaction could influence the initiation and progression of epidemics (Hilker and Schmitz 2008). For instance, resource limitation can reduce host density and thus disease risk, since for many directly and environmentally transmitted parasites, the well-known invasion threshold $\mathcal{R}_0$ (Anderson and May 1991) is proportional to the disease-free susceptible population size. Conversely, host–resource interactions that boost host density might promote disease spread. These possibilities mean that host and resource traits affecting their interaction may be pivotal for host–pathogen dynamics. Host–resource interactions may also shape disease epidemics when per-capita epidemiological traits depend on resource density. Such resource dependence of disease traits arises commonly. For instance, resources have been found to influence the production of parasites by an array of infective invertebrate hosts (mosquitoes–parasites: Bedhomme et al. 2004; Tseng 2004, 2006; *Daphnia*–parasites: Ebert et al. 2000, 2004; Bittner et al. 2002; Pulkkinen and Ebert 2004; Hall et al. 2009c, 2009a; ladybirds–mites: Ryder et al. 2007; monarch butterflies–protozoans: de Roode 2008; snails–trematodes: Johnson et al. 2007). Resource quantity and quality can also influence transmission rate (Keating et al. 1990; Hunter and Schultz 1993; D'Amico et al. 1998; Dwyer et al. 2005; de Roode et al. 2008; Hall et al. 2007, 2009c). Both of these traits—parasite production and transmission rate—can critically alter invasion success of parasites and the timing and dynamical behavior of epidemics (Keeling and Rohani 2008). Thus, from both a theoretical and empirical standpoint, we need to know if resource dependencies of these traits can alter disease dynamics.

Here, we tackle both of these issues using mathematical models that fuse consumer–resource theory with epidemiological theory. We start with the classic Rosenzweig–MacArthur model of consumer–resource dynamics (Murdoch et al. 2003). It provides an ideal foundation because it incorporates reasonable biology in the form of logistic resource growth and a saturating functional response of the host, while yielding both steady-state and cycling dynamics. Then, we layer in a parasite that infects the consumer (hereafter referred to as the host) and that is an "obligate killer," i.e., it produces infectious spores after killing the host (Ebert and Weisser 1997). This choice reflects the biology of a focal resource–host–parasite system: The host *Daphnia dentifera* is a small (1–2 mm) and abundant filter feeder whose population dynamics are strongly linked to its algal resource (Tessier and Woodruff 2002). These *Daphnia* species become infected with the virulent fungus *Metschnikowia bicuspidata* by ingesting infectious spores while feeding. The parasitic fungus grows inside the host until killing it and thereby releasing more infectious spores into the environment. Two key epidemiological processes in this system depend on algal density. First, the transmission rate decreases with resource density since contact with infectious spores increases with foraging effort (rate of filter feeding, water volume per unit time), and foraging effort decreases with increasing resource density (Hall et al. 2007). Second, the per-host yield of infectious spores increases with resource density, due to energetic and perhaps immune mechanisms (Hall et al. 2009c, 2010) as shown in Fig. 1F of Hall et al. (2009a). We present analytical and computational results describing the relevant consumer–resource and disease dynamics of this four-dimensional model and of a related three dimensional model applicable to directly transmitted diseases.

We find that the occurrence of host–resource cycles can inhibit parasite invasion when transmission is density-dependent (cf. Hilker and Schmitz 2008), in some cases leading to Allee effects (bistability) for the parasite. This Allee effect arises from host density-dependent transmission rates, and a "hydra effect" in the underlying consumer–resource model, i.e., increased mortality increases mean population size (Abrams 2009 and see Appendix D). Meanwhile, disease can modify and even stabilize host–resource cycling. Finally, our results show that resource dependence in epidemiological parameters can modulate these various dynamics. Resource dependence does not appear to affect the range of possible qualitative behaviors. However, it can have very strong quantitative effects, for example, on the ranges of parameters leading to cycling, steady-state persistence, and extinction of the parasite.

Model framework

To model the algae–*Daphnia*–*Metschnikowia* system and to achieve our ultimate goal of comparing model dynamics with and without resource dependencies in key epidemiological rates, we begin with a Rosenzweig–MacArthur consumer–resource model. We then incorporate an SIZ (S = susceptible, I = infected, Z = contagion) model of disease transmission among consumers. We have relaxed the traditional assumption that the per-capita transmission rate and spore production rates are constant and instead allow each

to depend on resource abundance. That is, we allow what are classically considered constant epidemiological parameters to be functions of resource abundance. Our general model is obtained by leaving those functions, and the functional form of the predation rate, unspecified. This approach allows us to address specific questions about our motivating biological system and to obtain results that apply to similar systems.

For clarity and mathematical tractability, we also consider a simplified, limiting case of the general model that is equivalent to assuming an SI disease model, where transmission occurs via direct contacts. This reduced model (Appendix B) has very similar dynamics to the general model and is studied here to help clarify certain results.

General model

The model tracks changing densities of the resource, n, susceptible consumers (herein "hosts"), x, infected hosts, y, and infectious contagion (e.g., fungal spores), z, which are dispersed in the environment. For clarity, we scaled the variables (see Appendix B) so that all population units are in resource equivalents (except a factor $\sigma(n)$ for spore density, z), and time has been scaled by the inverse of the consumer mortality rate (i.e., the average consumer lifetime in the absence of predation and disease). Our model resembles similar disease models that have been developed for this and other systems (Duffy et al. 2005; Hall et al. 2006, 2007; Duffy and Hall 2008; Hilker and Schmitz 2008) and is given by Eqs. 1a–1d:

$$\frac{dn}{dt} = rn(1-n) - \alpha(n)(x+y)n \tag{1a}$$

$$\frac{dx}{dt} = \alpha(n)(x+fy)n - (1+m)x - \beta(n)xz \tag{1b}$$

$$\frac{dy}{dt} = \beta(n)xz - (1+m\theta+v)y \tag{1c}$$

$$\frac{dz}{dt} = \sigma(n)(1+v)y - \mu z. \tag{1d}$$

In the absence of hosts, the resource follows a logistic growth model (Eq. 1a). Both infected (y) and uninfected hosts (x) feed on the resource at the same per-capita rate $\alpha(n)$, which for *Daphnia* we assume to yield a type II functional response. Susceptible (x, Eq. 1b) and infected (y, Eq. 1b) hosts consume those resources, but infected hosts suffer reduced fecundity ($0 < f < 1$; Hall et al. 2009a). Hosts die at a background rate scaled to rate 1, and due to predation at rate m. However, predation pressure is more intense for infected hosts, who die at rate θm, due to selectivity behavior of predators (i.e., $\theta > 1$; Duffy and Hall 2008). Susceptible hosts become infected at per-capita rate $\beta(n)$ as they contact spores distributed in the environment (z, Eqs. 1b and 1c). Motivated by empirical observations, the transmission rate $\beta(n)$ can depend on resource density, n, as described below or can remain constant ($\beta(n) = \beta$). Infected hosts that die from causes other than predation (at rate $1 + v$) release spores into the environment at rate $\sigma(n)$, which can also depend on resource density. Spores experience their own loss from the environment at rate μ. Other epidemiological and demographic rates, e.g., rates of disease progression and host reproduction (Hall et al. 2009a), may also be resource- or disease-status-dependent, and these may vary among different host–parasite systems. Here, we restrict our focus to resource-dependent transmission and spore production.

For some analyses, we need to specify functional forms for the feeding rate $\alpha(n)$, transmission rate $\beta(n)$, and spore yield $\sigma(n)$. Our most general results only require that these functions are positive and differentiable. Based upon empirical results for the *Daphnia–Metschnikowia* system in particular, these specific functions are

$$\alpha(n) = \frac{a}{k+n} \tag{2a}$$

$$\beta(n) = \frac{\beta_c}{k+n} \tag{2b}$$

$$\sigma(n) = \sigma_0 \cdot (1+\phi n). \tag{2c}$$

The per-resource, per-host feeding rate $\alpha(n)$ (Eq. 2a) assumes a type II feeding rate with maximal consumption rate a and a half-saturation parameter k. The host's "clearance rate" is the volume of habitat from which the resource (and spores) is removed per unit time (Grover 1997), and this measure of foraging effort is proportional to $\alpha(n)$. Since the clearance rate drives contact with infectious spores, we require that the per-spore, per-host transmission rate $\beta(n)$ (Eq. 2b) be proportional to the clearance rate and likewise decline with increasing resource density. Parameter β_c is the maximal infectivity of spores once contacted. Based upon the data described by Hall et al. (2009a), spore yield $\sigma(n)$ is assumed to increase with resource density (with positive intercept σ_0 and slope $\phi\sigma_0$, see Appendix C for details).

Model parameters and methods of analysis

Parameters values for Eq. 1 (see Appendix C) mostly come from previous empirical studies (Hall et al. 2006, 2007; Duffy et al. 2005; Duffy and Hall 2008). In some cases, broad parameter ranges were chosen to explore a range of possible dynamics. This is consistent with the broad-range variability found in natural systems, particularly regarding algal growth rates and maximum densities.

The model dynamics were analyzed using standard methods of equilibrium stability analysis and bifurcation theory, as detailed in the appendices and online-only supplement. Computational results were obtained through simulation

and by using the bifurcation continuation software MATCONT in MATLAB.

One nonstandard aspect of our analysis merits special note. We sought to compare bifurcation diagrams between different versions of these models with either constant (resource-independent) or resource-dependent rates of transmission $\beta(n)$ and spore production $\sigma(n)$. These differences, however, also yield different equilibrium population sizes. Importantly, equilibrium population size partly determines equilibrium stability. Thus, to ensure proper comparison of model dynamics, we correct for this by using "equilibrium matching." We parameterize each model so that their equilibrium population sizes are equal. Specifically, the parameters in Eq. 2 were set to

$$a = (k + n_*)\alpha \tag{3a}$$

$$\beta_c = (k + n_*)\beta \tag{3b}$$

$$\sigma_0 = \frac{\sigma}{1 + \phi n_*} \tag{3c}$$

so that $\alpha(n_*) = \alpha$, $\beta(n_*) = \beta$, and $\sigma(n_*) = \sigma$ (see Figs. 1 and 2). The equilibrium value n_* used in our analyses is the resource–host–parasite coexistence equilibrium n_2, unless stated otherwise (see Appendix S1 for details).

Results

We begin our analysis with a review of the host–resource dynamics in the absence of disease and of the conditions for parasite invasion into a disease-free system. We then use bifurcation analysis to determine the range of possible dynamics in the model with constant (resource-independent) epidemiological parameters and contrast this with the dynamics when the disease transmission rate $\beta(n)$ and spore production rate $\sigma(n)$ are resource-dependent.

Much of these dynamics are expected, i.e., they follow naturally from the dynamics of the underlying consumer–resource and disease transmission models. However, these models also exhibit additional unexpected dynamics, specifically instances of bistability. We provide a brief, intuitive explanation of why such phenomena arise in this system, and similar models of tri-trophic food webs, but not in similar disease systems where transmission is frequency-dependent.

To discuss these dynamics, we use the following notation for periodic (limit cycle) and equilibrium solutions to these models. The endemic disease steady state is denoted

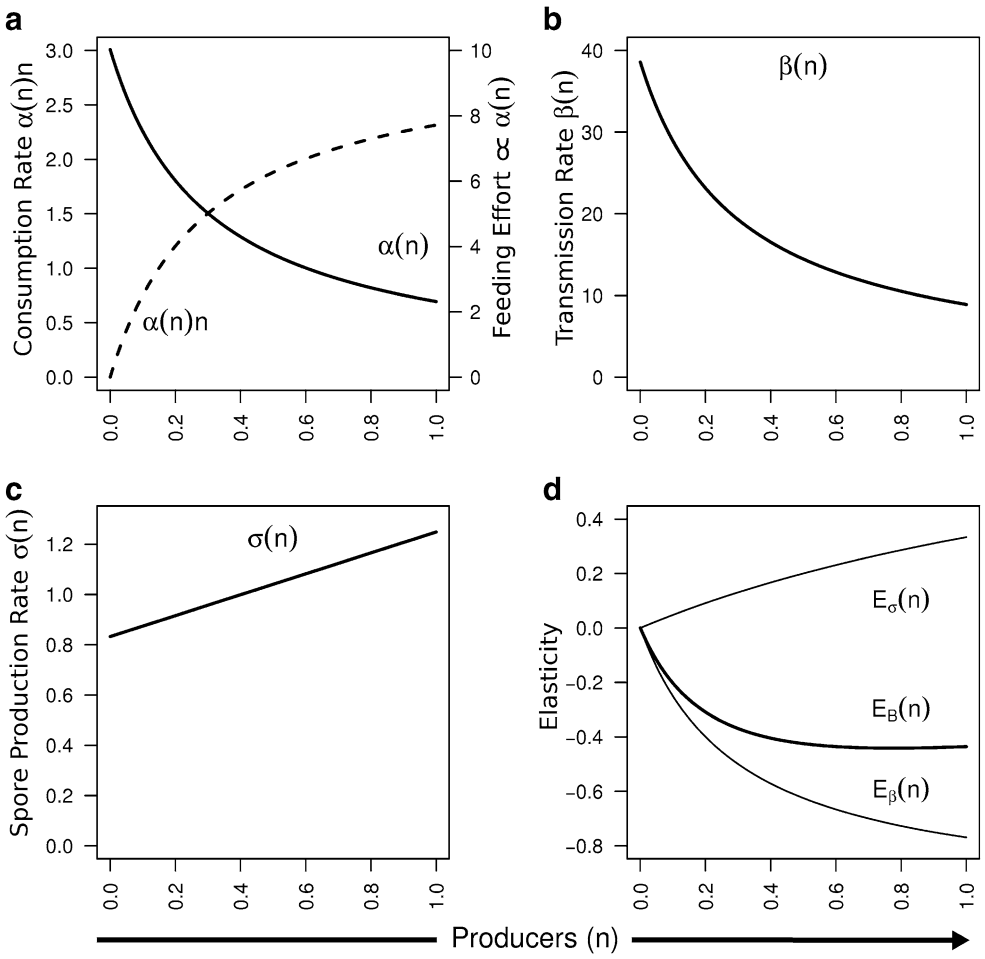

Fig. 1 Examples of resource (n)-dependent consumption rate, $\alpha(n)$ (**a**), transmission rate $\beta(n)$ (**b**), and spore yield $\sigma(n)$ (**c**), and their elasticities (**d**). (**a**): A type II consumption rate $\alpha(n)n$ implies that the rate of environmental exposure to spores of the parasite (e.g., clearance rate, or volume of water filtered per unit time) is proportional to $\alpha(n)$. (**b**): This rate of exposure implies that transmission rate $\beta(n)$ is proportional to $\alpha(n)$. Thus, transmission rate decreases with resource density. (**c**): Spore yield $\sigma(n)$ increases linearly with resource density. (**d**): Incorporating resource-dependent rates $\beta(n)$ and $\sigma(n)$ will shift the Hopf bifurcation curve. Whether this shift expands or shrinks the parameter region corresponding to stable resource–host–parasite dynamics depends (approximately) on whether $B(n)$ (Eq. 5) is increasing or decreasing, respectively, at the endemic equilibrium $n = n_2$. See the main text and online supplement for additional details

as $EQ_2 = (n_2, x_2, y_2, z_2)$. The disease-free host–resource steady state EQ_1 and the resource-only steady state EQ_n are as defined above. We refer to the asymptotically stable resource–host–parasite cycles as LC_2 and the disease-free host–resource cycles as LC_1. See Appendix S1 for further details.

Consumer–resource dynamics and parasite invasion

The general consumer–resource (hereafter *host–resource* or *disease-free*) model implicit in Eqs. 1a and 1b is well understood (e.g., Murdoch et al. 2003 and see our Appendix S1). This subsystem produces either host–resource coexistence at steady state (we denote this disease-free equilibrium $EQ_1 = (n = n_1, x = x_1)$) or a stable resource-only equilibrium $EQ_n = (n = 1, x = 0)$, depending on the host's basic reproduction number,

$$\mathcal{R}_{0c} = \frac{\alpha(1)}{1+m}. \tag{4}$$

The quantity $\mathcal{R}_{0c}$ is the expected lifetime number of new hosts produced per individual under ideal conditions (i.e., at the resource-only boundary when resource density is maximal). When $\mathcal{R}_{0c} > 1$, the host can invade the resource-only equilibrium. If the feeding rate is linear (constant $\alpha(n) = \alpha$), the host–resource coexistence equilibrium is globally stable. However, when the feeding rate saturates according to a type II functional response (i.e., Eqs. 2a and 3a), the host–resource system is the well-known Rosenzweig–MacArthur model (see Fig. 2) which permits host–resource cycling. These oscillations arise via the famous "paradox of enrichment" (Rosenzweig 1971) or, alternatively framed, the "suppression–stability trade-off" (SST) (Murdoch et al. 2003) which is the perspective used in this article. Figure 2 shows this transition to cycling, in the context of the SST, and illustrates how bifurcation diagrams of these dynamics can by interpreted similarly, whether we use standard model parameters (Fig. 2a) or equilibrium matching (Fig. 2b). Biologically, cycling starts due to an increase in the maximum resource availability (i.e., producer carrying capacity) and/or an increase in the effectiveness (efficiency of consumption, low k, or high maximal consumption rate α) of hosts. Mathematically, the transition to cycling comes from a Hopf bifurcation, as detailed in Appendix S1. For our purposes, it suffices to say that the host–resource dynamics are more likely to oscillate with efficient hosts with high consumption rates $\alpha(n)$. As expected, the underlying consumer–resource model drives steady-state and cycling host population dynamics in the presence of disease.

Whether or not the parasite can invade a disease-free steady state depends on whether the basic reproduction number for disease, $\mathcal{R}_{0d}$, is greater than or less than 1. If we define

$$B(n) = \frac{\beta(n)\sigma(n)(1+\nu)}{\mu}, \tag{5}$$

then for all models considered,

$$\mathcal{R}_{0d} = \frac{B(n_1)x_1}{1+\nu+m\theta}. \tag{6}$$

This can be interpreted as the expected number of new infections per infected individual in a disease-free population. We therefore expect to see disease invades a

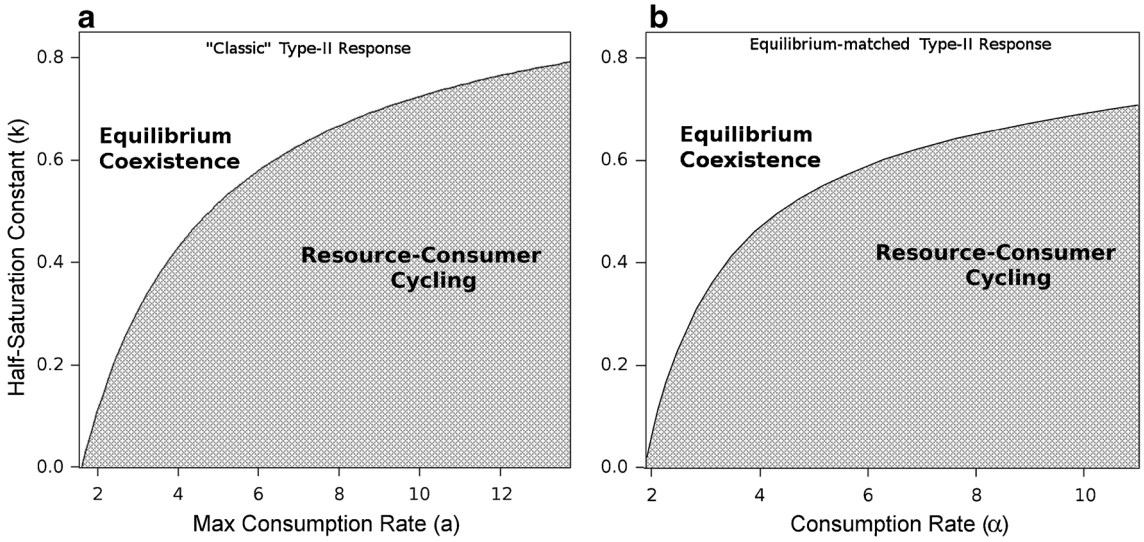

Fig. 2 Disease-free consumer–resource dynamics of model (1) assuming a type II consumption rate with either (panel **a**) no equilibrium matching ($\alpha(n) = a/(k+n)$, Eq. 2a) or with equilibrium matching (panel **b**, Eq. 2a with Eq. 3a). These two cases illustrate how the interpretation of bifurcation diagrams is largely unaffected by equilibrium matching. Parameters used: $r = 40$, $f = 0.75$, and $m = 0.6$

disease-free host–resource steady state when both $\mathcal{R}_{0c}$ and $\mathcal{R}_{0d}$ are greater than 1. Threshold conditions for parasite invasion of a disease-free host–resource limit cycle LC_1 cannot be given analytically. However, for the limiting case of our model, where transmission is effectively contact-based instead of spore-based (spore turnover is assumed to be fast, see Appendix D), the parasite can invade disease-free cycles LC_1 if

$$\frac{\langle B(n_1)x_1\rangle}{1+\nu+m\theta} > 1 \tag{7}$$

where $\langle\cdot\rangle$ denotes the average value over the disease-free limit cycle LC_1.

Dynamics of the constant rates models

The nature of the dynamics described above can be more succinctly summarized, and compared between models, using bifurcation diagrams. Figures 3 and 4 illustrate these dynamics. Consider first the dynamics exhibited by the general model (Eq. 1) with constant transmission rate $\beta(n) = \beta$ and spore yield $\sigma(n) = \sigma$. The bifurcation diagram in Fig. 4 summarizes the dynamics of this model over a range of different parameter values related to the predation efficiency of the hosts, which increases with increasing α and decreasing k. Each region ①–⑤ contains parameter values that yield the corresponding dynamics described above, and the boundaries between those regions are characterized

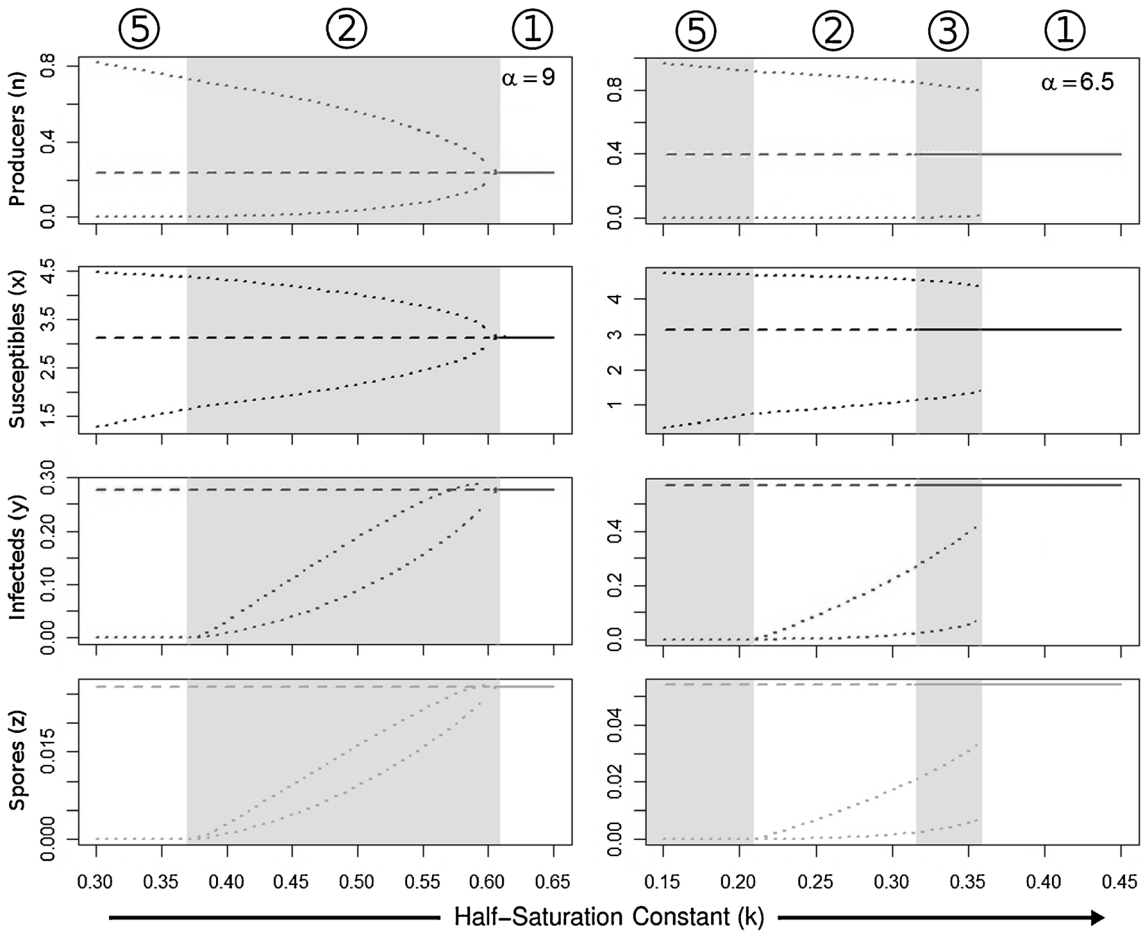

Fig. 3 Examples of how the model dynamics change as parameters are varied along two different paths through the bifurcation diagram in Fig. 5d. *Shading* indicates different regions separated by bifurcations. See Fig. 4 for region ①–⑤ definitions and bifurcation details. *Solid lines* indicate that the three-species steady state (EQ_2) is (locally) stable; *dashed lines* indicate that it is locally unstable; and *dotted lines* mark the minimum and maximum values of stable limit cycles with disease (LC_2) or without (LC_1). As the half-saturation constant (k) increases, hosts become less efficient consumers. On the *left* ($\alpha = 9$), as k increases, cycle amplitude is reduced and mean population size *increases*, permitting parasite invasion. Combined with increased disease mortality, this eventually stabilizes cycling. On the *right* ($\alpha = 6.5$), the nonlinear increase in mean host density (not shown) permits a region of bistability between resource–host–parasite cycling (LC_2) and steady-state coexistence (EQ_2) as discussed in the text and Appendix D. Though not shown, in ③, there is an unstable limit cycle (LC_u) that is part of the separatrix between basins of attraction for the two bistable states

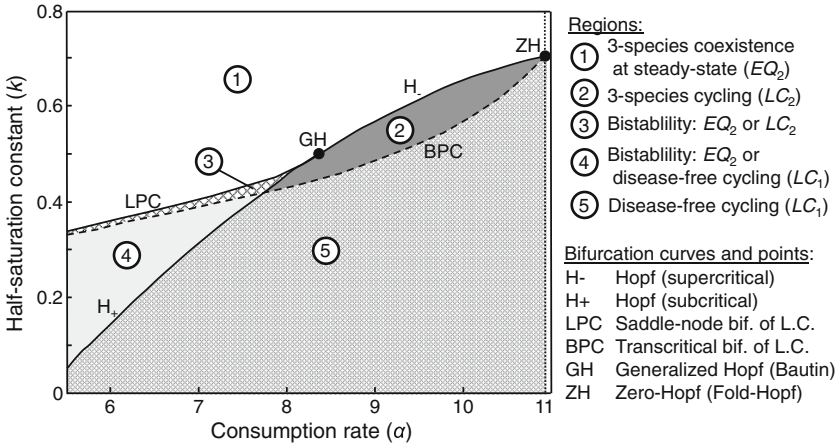

Fig. 4 A bifurcation diagram summarizing the five different behavioral regimes (see Fig. 3) of model (1) with constant transmission rate β and spore yield σ. The bifurcations are plotted over a range of two key traits of the host's type II functional response-based feeding effort (see Eqs. 2a and 3a): equilibrium matched consumption rate α and half-saturation constant k. For a bifurcation summary, see Appendix A. See Appendix A for description of other bifurcations that could arise. Parameters used: $r = 40$, $f = 0.75$, $m = 0.6$, $\theta = 9$, $\nu = 1$, $\mu = 19$, $\beta = 25$, and $\sigma = 0.9$

by different types of bifurcations. Figure 3 illustrates these dynamics along the vertical paths at $\alpha = 6.5$ and $\alpha = 9$ in Fig. 4 (under the resource-dependent model). Additionally, less biologically relevant dynamics can occur in the parameter regions shown, but for clarity, we have omitted these cases (see Appendix A for details).

In region ①, the endemic disease equilibrium EQ_2 is stable: disease persists in the host–resource system without population oscillations. In some parts of this region, disease-free initial conditions lead to disease-free host–resource cycling, which is otherwise stabilized by disease-induced mortality (see Fig. 4 and compare with Fig. 2). In region ②, the stable interior equilibrium EQ_2 has lost stability via a supercritical Hopf bifurcation (labeled H_-), causing the system to exhibit resource–host–parasite cycles LC_2 (see Fig. 3 for equivalent dynamics). In region ⑤, the disease is unable to persist due to low average population density (see Eq. 7) and the system exhibits asymptotically stable disease-free host–resource cycles LC_1. Regions ③ and ④ are regions of bistability between the endemic disease equilibrium EQ_2 and cycling dynamics. That is, different initial conditions will either lead to the endemic disease steady state EQ_2 or will lead to host–resource cycling with (region ③, LC_2 stable) or without (region ④, LC_1 stable) disease.

This bistability (regions ③, ④) is absent from a similar system with frequency-dependent, instead of host-density-dependent, disease transmission (Hilker and Schmitz 2008). To intuit why density-dependent transmission yields bistability, consider the average host population size during host–resource cycling. The Rosenzweig–MacArthur model exhibits a *hydra effect* (Abrams 2009) in the cycling regime: increased mortality leads to a resource-mediated increase in average population size. Parasites, by increasing host mortality and thus host density, facilitate their own transmission, producing a strong Allee effect for the parasite (see Appendix D for details).

The dynamics illustrated in Fig. 3 and summarized in Fig. 4, particularly the nature of the bistability in regions ③ and ④, can be understood by considering the generic dynamics near a generalized Hopf bifurcation (GH and curves H_+, H_-, and LPC in Fig. 4) combined with the loss of parasites at the transcritical bifurcation of limit cycles, BPC. A brief summary of these bifurcations can be found in Appendix A.

Dynamics with resource-dependent epidemiological processes

We can now address how resource-dependent rates of susceptibility (transmission rate $\beta(n)$) and infectiousness (spore yield $\sigma(n)$) affect two key features of the dynamics described above: the tendency for the system to cycle and the ability of parasites to persist in the host population. To accomplish this, we first consider how resource-dependent epidemiological processes affect the parasite's ability to invade a disease-free population by considering their impact on $\mathcal{R}_{0d}$. Second, we compare bifurcation diagrams for the constant (resource-independent)–rate model described above and in Fig. 4 and for the variable (resource-dependent)–rates model with nonconstant transmission rate $\beta(n)$ and spore production rate $\sigma(n)$. Specifically, we focus on the transition between steady-state and cycling dynamics marked by the Hopf bifurcation curve H and the loss of disease from the three-species cycles marked by BPC.

The resource dependence of $\mathcal{R}_{0d}$ (Eq. 6) has two noteworthy implications: First, the shape of that dependence

(i.e., of $\beta(n)$ and $\sigma(n)$) may skew this classical relationship between basic reproduction number $\mathcal{R}_{0d}$ and $s_2 = x_2/x_1$, i.e., the number of susceptibles at the endemic equilibrium (x_2) relative to the number at the disease-free state (x_1). That is, classically, $\mathcal{R}_{0d} = 1/s_2$; however, with resource-dependent transmission ($\beta(n)$) and spore yield ($\sigma(n)$), $\mathcal{R}_{0d} = \frac{B(n_1)}{B(n_2)}\frac{1}{s_2}$. That is, ignoring resource-dependent epidemiological processes may bias inferences based on epidemic data. Second, host populations in strongly seasonally forced environments experience substantial resource fluctuations. Therefore, efforts to estimate disease risk (i.e., $\mathcal{R}_{0d}$) from population data (e.g., Cintrón-Arias et al. 2009) may benefit from including known resource dependencies.

Beyond these effects on $\mathcal{R}_{0d}$, resource-dependent epidemiological processes can further affect parasite persistence and the tendency for the system to cycle, as illustrated in Fig. 5. Here, we consider the isolated (Fig. 5b, c) and combined (Fig. 5d) effects of resource-dependent $\beta(n)$ and $\sigma(n)$, in particular, how each affects the location of the Hopf bifurcation curve H (i.e., the tendency of the system to cycle) and the size of regions ② and ③ (i.e., parasite persistence under cycling dynamics).

Resource-dependent epidemiological rates can either shrink or expand the region of parameter space that yield steady-state dynamics (region ① as well as ③ and ④) by shifting the Hopf bifurcation curve in parameter space (recall Fig. 2). In general, we can predict the direction of this shift using the slopes (i.e., derivatives) of the resource-dependent rate functions, $\sigma'(n)$ and $\beta'(n)$, but stated in terms of their elasticities, which are defined as follows: For a given function, $F(n)$, the elasticity of F with respect to n is a dimensionless quantity that represents the proportional change in $F(n)$ per proportional change in n and is defined as $E_F \equiv F'(n)\frac{n}{F(n)}$. Two key properties of elasticities are used below: First, the elasticity E_F and derivative $F'(n)$ have the same sign whenever the values $F(n)$ and n are positive. Second, if function F is proportional to the product of two functions, e.g., $F(n) \propto g(n)h(n)$, then elasticity of that function is the sum of the elasticities of functions g and h: $E_F = E_g + E_h$ (see Fig. 1). Lastly, we denote elasticities evaluated at the endemic-disease steady-state (EQ_2) resource density (n_2) with an asterisk, e.g., E_{F*}.

The shift in the location of the Hopf curve H (relative to resource-independent case with constant β and σ, i.e., constant direct transmission rate, Eq. 5) will either shrink or expand the regions of steady-state three-species coexistence. To interpret the criteria for whether this region shrinks or expands, we first consider the limiting case of our model that assumes fast spore turnover (see Appendix B). For this simplified model, the direction of the shift depends on the sign of the net elasticity E_{B*} (i.e., the elasticity of the direct transmission rate $B(n)$; see Eq. 5 and Fig. 1), given by

$$E_{B*} = E_{\beta*} + E_{\sigma*}. \tag{8}$$

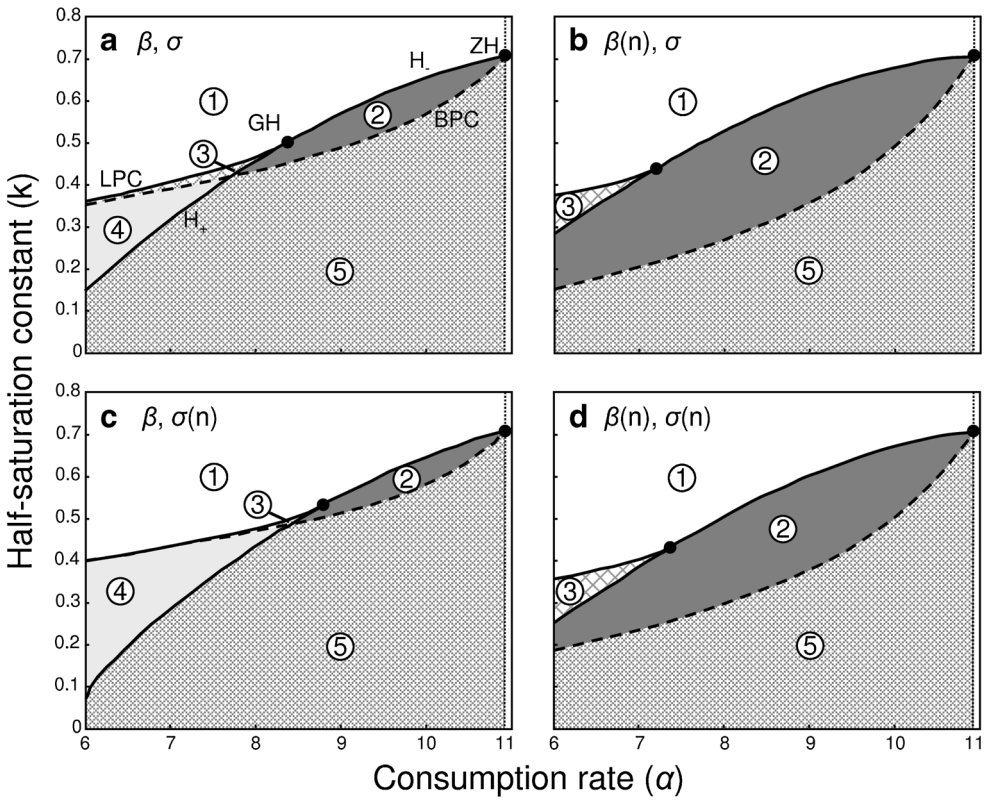

Fig. 5 Comparison of model (1) dynamics with constant and resource-dependent rates of transmission $\beta(n)$ and spore production $\sigma(n)$. Panel **a** shows the same constant–rates model diagram as in Fig. 4. Panels **b** and **c** show the diagrams for model (1) with resource dependence in either $\beta(n)$ or $\sigma(n)$, but not both. In panel **d**, both rates are resource-dependent. See Fig. 4 for examples of the dynamics in each parameter region. See Appendix A for definitions and a summary of the bifurcations, and see Appendix A for additional dynamics not shown in these diagrams

If E_{B*} is positive (i.e., if $B(n)$ is increasing at n_2), H will occur at lower k values, thus expanding the range of steady-state three-species coexistence. If E_{B*} is negative (i.e., $B(n)$ decreasing at n_2), this region of steady-state coexistence will shrink (see Appendix S2 for details).

Importantly, this biologically intuitive criterion also approximately holds for the general model (Eq. 1). Applying this result to our motivating *Daphnia–Metschnikowia* example (see Figs. 1 and 5a, d), the net resource dependence is negative, suggesting an upwards shift in the Hopf bifurcation H and thus a reduced set of parameters leading to steady-state three-species coexistence. Moreover, the criteria imply that a decreasing transmission rate $\beta(n)$ destabilizes the system (i.e., increases the tendency to cycle; Fig. 5b) while the increasing spore yield $\sigma(n)$ stabilizes it (i.e., decreases the tendency to cycle; Fig. 5c).

The exact criterion for the general model (Eq. 1) is the same as in the reduced model (Eq. B2) if spore yield alone is resource-dependent: If $\sigma(n)$ increases with resource density n, this will stabilize the dynamics (i.e., expand the region of EQ_2 stability, as is the case with the direct transmission model). If transmission rate $\beta(n)$ is resource-dependent, the exact criteria for the general model are less intuitive but can be computed (see Appendix S2 for details). If spore dynamics are fast (e.g., when spore loss rate, μ, and spore yield, σ, are relatively large), then this criterion (for the general model, Eq. 1) agrees with the criteria for the reduced model (Eq. 8).

Resource-dependent epidemiological processes also affect nonequilibrium population dynamics, including parasite–host–resource cycling as illustrated in Fig. 5. There we see disease is lost from host–resource cycling as we cross the transcritical bifurcation of limit cycles, BPC. Here, the invasion criteria Eq. 7 drops below 1, and disease can no longer invade the disease-free cycle LC_1. Comparing resource-dependent and resource-independent cases, we see that resource-dependent spore yield $\sigma(n)$ given by Eq. 2c inhibits parasite persistence during host–resource cycling, as indicated by the reduced sizes of regions ② and ③ (compare a and c in Fig. 5). This is because, at higher overall consumption rates (higher α), average resource levels are driven down. According to Eq. 2c, this reduces the spore yield of infected hosts. This diminished ability to invade would be reversed if $\sigma(n)$ was instead a decreasing function of resource density n. In contrast, a resource-dependent transmission rate $\beta(n)$ (compare a and b in Fig. 5) has the opposite effect. Low average resource levels during host–resource cycling yield an increase in infectiousness by increasing the contact rate via increased foraging activity. This offsets the consequences of low average host density and allows increased parasite persistence. For our motivating example (Fig. 5d), the effects of $\beta(n)$ outweigh those of $\sigma(n)$, resulting in a slight increase in the tendency to cycle and a large increase in the range of parasite persistence during nonequilibrium dynamics.

Discussion

Trophic interactions and disease processes commonly interact in nature, yet theory that combines the two remains relatively scarce. The results presented here show how these two forces jointly shape the dynamics of parasitized consumer populations. In particular, host–resource (consumer–resource) dynamics can profoundly affect the invasion and persistence of parasites in host populations, and disease-related mortality can greatly affect host population dynamics. Moreover, we have shown that these host–parasite dynamics can be altered when key epidemiological traits of hosts depend directly on resource abundance, i.e., the transmission rate $\beta(n)$ and contagion (spore) production rate $\sigma(n)$). While the dynamic repertoire remains qualitatively intact, important quantitative features of these dynamics can vary greatly. These results can be applied to systems with related resource dependencies, and our approach can be followed to investigate other host–parasite systems where epidemiological and demographic rates may be resource- or disease-status-dependent.

To detail these findings in the preceding sections, we focused on the key bifurcations that summarize these three species dynamics across a range of host traits central to the suppression–stability trade-off (i.e., the paradox of enrichment: Murdoch et al. 2003). We then compared those dynamics between models with and without these resource dependencies. This discussion is similarly organized: First, we highlight some noteworthy insights from the dynamics of the three-species models and then discuss the role of resource-dependent epidemiological processes in that context.

Resource–host–parasite dynamics

The three-species dynamics exhibited by models Eqs. 1a–d and B2a–c include host–resource (consumer–resource) cycling, with and without parasite persistence, and instances of bistability between the endemic (three-species) steady state and cycling with or without parasites. These dynamics occur near a generalized Hopf (Bautin) bifurcation, which likely occur in similar three-species food web models. In situations of bistability between endemic disease and disease-free host–resource cycles, there is an Allee effect for the parasite: it can persist when it is abundant, but cannot invade when it is rare. This Allee effect arises from (1) increased mortality from disease, (2) a hydra effect (increased mortality increases population size; Abrams 2009) whereby average host density *increases* with mortality (see Appendix

D; also Matsuda and Abrams 2004; Sieber and Hilker 2011), and (3) density-dependent transmission (cf. Hilker and Schmitz 2008). Parasite spread during host–resource cycling requires a sufficiently high *average* host density to invade and create endemic disease (see Appendix D for an extension of the well-known $\mathcal{R}_0 > 1$ criterion; Anderson and May 1991; Keeling and Rohani 2008). During large-amplitude cycles, average host density can be quite low (Appendix D; Armstrong and McGehee 1980; Murdoch et al. 2003)—too low to support parasites. However, increased mortality from infection during host–resource cycling reduces this tendency for host populations to cycle and simultaneously increases average host density via the hydra effect. Thus, since parasite transmission here is host-density-dependent, the parasite facilitates its own invasion of cycling host populations (Appendix D).

These results predict that host–resource cycling can exclude parasites if mean host density becomes too low. Importantly, host–resource cycling requires hosts that are efficient consumers, i.e., they exhibit sufficiently high feeding rates α or low half-saturation constants k. Interestingly, this applies to fast-feeding and efficient hosts that might otherwise be expected to support parasites because of a high transmission rate (i.e., a high probability of contacting spores). Additionally, we predict the Allee effect for parasites invading cycling host populations to only occur if parasite transmission rates are host-density-dependent. This Allee effect is not expected if transmission is frequency-dependent (Hilker and Schmitz 2008) since increased average host density would not lead to an increased transmission rate. Allee effects can also occur in host–pathogen systems through other mechanisms, including nonlinear transmission rates, host immune responses, local spatial interactions, demographic stochasticity, predation, and positive density dependence in hosts (e.g., Holmes 1997; Gubbins et al. 2000; Regoes et al. 2002; Hall et al. 2005; Hilker et al. 2009).

As we have shown, the underlying host–resource system promotes cycling dynamics of disease, and disease can strongly dampen (and even stabilize) host–resource cycling. These results echo those revealed from a resource–host–parasite system with different underlying epidemiology (Hilker and Schmitz 2008). When hosts are highly efficient consumers (high feeding rates α or low half-saturation constants k), they induce host–resource cycling. If such a system is far from the Hopf bifurcation, or if disease-induced mortality is limited, parasite prevalence will cycle as host density cycles (Hilker and Schmitz 2008; Appendix D). This result helps to explain why disease might fluctuate in natural systems (Hethcote and Levin 1989; Greenman and Hudson 1997). Typically, mechanisms to explain disease cycles depend on seasonal forcing or specific epidemiological details (Hethcote 1973; London and Yorke 1973; Anderson and May 1981; Hethcote et al. 1981; Liu et al. 1986) or Allee effects in the underlying host dynamics (Hilker et al. 2009). Again, here we see that host–resource cycling, like predation (Dwyer et al. 2004; Hall et al. 2005), can stimulate oscillations in disease. Higher levels of disease-induced mortality, however, allow parasites to essentially push the underlying host–resource systems from cycling to stable steady-state behavior. Thus, parasitism might help to explain why some natural host–resource systems often cycle less than predicted by simpler but reasonable consumer–resource models without disease (McCauley and Murdoch 1990; Kirk 1998; McCauley et al. 1999; Jensen and Ginzburg 2005).

Resource-dependent disease processes

Incorporating resource-dependent epidemiological traits in these models had a big impact on some important quantitative aspects of these dynamics, despite yielding limited qualitative differences. In general, resource-dependent epidemiological traits of hosts can either stabilize or destabilize three species cycling dynamics. We concluded that, for the most part, both traits typically stabilize dynamics when they increase with resource density, but destabilize them when they decrease with density (Eq. 8). When these traits oppose each other (e.g., transmission rate decreases while spore yield increases with produce density, as in the motivating *Daphnia* system: Hall et al. 2007, 2009c, b, 2010), their combined effect on stability can be calculated for a broad family of models as illustrated in Fig. 1. Using parameter values and functional forms from the *Daphnia* system, resource-dependent transmission rate exerted the strongest, destablizing effects on resource–host–parasite dynamics. Additionally, this resource-dependent transmission rate greatly expanded the region of parameter space that permitted parasite invasion of host–resource cycles. This suggests that, for host populations that experience variable resource dynamics, the occurrence and severity of epidemics could be substantially altered by resource dependence in key epidemiological processes (even if host population size remains constant). Together, these results underscore the importance of uncovering and quantifying third-party dependencies among traits that affect pairwise interspecific interactions within communities and the importance of developing theory to predict the population and community level consequences of those dependencies.

In general, this study starkly illustrates how host ecology can shape the dynamics of disease epidemics, but it also provides a foundation for multiple avenues of future research. For instance, these models can exhibit still more kinds of dynamics (see Appendix A), some of which may be relevant to other disease systems or tri-trophic food web models. Additionally, host populations could evolve during epidemics. Evolution of hosts in the *Daphnia* system

could intimately interact with these resource–host–parasite dynamics because feeding rate and epidemiological traits among clonal genotypes are mechanistically linked (Hall et al. 2010). Furthermore, the host–resource system often experiences (periodic) seasonal forcing. This forcing could change the underlying host–resource dynamics (Scheffer et al. 1997) and thereby alter disease dynamics. Moreover, host–resource interactions need to be more fully integrated into existing theory for the community ecology of infectious disease. For instance, some species compete with hosts for resources but remove parasites through a dilution effect (Norman et al. 1999; Keesing et al. 2006; Hall et al. 2009b). Also, predators indirectly influence consumer–host cycling and disease dynamics (Scheffer et al. 2000; Dwyer et al. 2004; Hall et al. 2005). Connecting host–resource interactions with the epidemiologically relevant processes like the dilution effect and predation may greatly enhance theory for both. Thus, we hope that the resource–host–parasite models studied here and elsewhere (e.g., Hilker and Schmitz 2008) play more central roles in future developments of theory for infectious disease.

Acknowledgments This article is based on the work in the lead author's doctoral dissertation (Hurtado 2012) submitted in partial fulfillment of the requirements for a PhD in Applied Mathematics at Cornell University. Paul J. Hurtado thanks the Mathematical Biosciences Institute at The Ohio State University (NSF DMS 06-35561, 09-31642) for hosting him during the writing of this manuscript. Spencer R. Hall was supported by NSF grants DEB 06-13510 and DEB 06-14316. Stephen P. Ellner was supported by grant 220020137 from the James S. McDonnell Foundation and US National Science Foundation grant DEB 08-13743.

Appendix A: Bifurcation summary

The dynamics illustrated in Fig. 4, particularly the bistability in regions ③ and ④, can be summarized as the generic dynamics near a generalized Hopf (Bautin) bifurcation with a nearby transcritical bifurcation of limit cycles BPC that correspond to the loss of parasites from the three-species cycles LC_2. A generalized Hopf bifurcation has three branches (see Fig. 4): a supercritical Hopf H_- (to the right of GH), a subcritical Hopf H_+ (to the left of GH), and a saddle-node bifurcation of limit cycles LPC (for *limit point cycle*). The nature of the bistability that arises between LPC and H_+, and the basins of attraction for each outcome, can be more clearly understood by considering the dynamics near these two bifurcation curves (also see Fig. 3). The subcritical Hopf H_+ gives rise to an unstable periodic orbit LC_u which exists for k values above H_+ in regions ③ and ④ and forms part of the separatrix that separates the basins of attraction between the three-species steady-state EQ_2 and the stable limit cycle in regions ③ (LC_2, parasites present) and ④ (LC_1, no parasites). Ignoring BPC for the moment, traversing ③ and ④ from H_+ towards LPC, the amplitude of the unstable cycle LC_u increases as it approaches the stable limit cycle. Continuing across LPC, the two cycles collide (forming a limit point cycle, where $LC_u = LC_2$, at LPC) then disappear, leaving only the stable disease equilibrium (EQ_2) as the lone attractor in region ①. As a result, the basin of attraction for the stable interior equilibrium, EQ_2, is vanishingly small near the subcritical Hopf bifurcation, H_+ (i.e., most trajectories result in cycling), while the basin of attraction for EQ_2 dominates near LPC. BPC separates regions ③ (cycling with disease) and ④ (without disease) and marks the threshold at which disease can no longer persist in the cycling host population.

Appendix B: Model derivation

The general model (Eq. 1) is a rescaled version of the following model, which is based on spore-based fungal parasitism of *Daphnia* sp. N is producer density (per liter), X is susceptible consumer density (per liter), Y is infected consumer density (per liter), Z is infectious spore density (spores per liter), and time τ is in days. Table 1 contains parameter descriptions, ranges, and values.

$$\frac{dN}{d\tau} = \tilde{r}N(1 - N/K) - \tilde{\alpha}(N)N(X + \rho Y) \tag{B1a}$$

$$\frac{dX}{d\tau} = \chi\tilde{\alpha}(N)N(X + \tilde{f}\rho Y) - (d_x + \tilde{m})X - \tilde{\beta}(N)XZ \tag{B1b}$$

$$\frac{dY}{d\tau} = \tilde{\beta}(N)XZ - (d_x + \tilde{\nu} + \tilde{m})Y \tag{B1c}$$

$$\frac{dZ}{d\tau} = \tilde{\sigma}(N)(d_x + \tilde{\nu})Y - \tilde{\mu}Z - \eta\tilde{C}(N)Z(X + \rho Y) \tag{B1d}$$

The rescaled model (Eq. 1) is given by $t = \frac{\tau}{\frac{1}{d_x}}$, $r = \frac{\tilde{r}}{d_x}$, $\alpha = \frac{\chi\tilde{\alpha}}{d_x}$, $k = \tilde{k}/K$, $f = \tilde{f}\rho$, $m = \frac{\tilde{m}}{d_x}$, $C = \eta\tilde{C}\chi K\frac{1}{d_x}$, $C_c = \eta\tilde{C}_c\frac{\chi}{d_x}$, $\beta = \tilde{\beta}\chi K\frac{1}{d_x}$, $\nu = \frac{\tilde{\nu}}{d_x}$, $\sigma = \tilde{\sigma}$, and $\mu = \frac{\tilde{\mu}}{d_x}$. This leaves the rescaled variables as $n = N/K$, $x = \frac{X}{\chi K}$, $y = \frac{Y}{\chi K}$, and $z = \frac{Z}{\chi K}$. We further simplify this model by assuming that consumption does not deplete spores in the environment, i.e., that $C \equiv 0$. See Table 2 for parameter descriptions.

Reduced model

Model (1) can be simplified by assuming that spore turnover is fast (σ, μ very large). In that case, spore density $z(t)$ tracks the equilibrium of Eq. 1d obtained by holding the density of infected hosts $y(t)$ constant, $z(t) = \left(\frac{\sigma(n(t))(1+\nu)}{\mu}\right)y(t)$. Substituting this expression for $z(t)$ into

Table 1 Parameter values and descriptions for the unscaled model

Parameter	Value	Range	Description
K	10^4	$10^2 - 10^9$	Algal carrying capacity (no. per liter) (Porter et al. 1982)
$\tilde{r}$	2	$0.69 - 2.8$	Algal growth rate (no. per day) (Sorokin and Krauss 1958)
$\tilde{a}$	3.16×10^2	$\approx \frac{1}{100d} - \frac{1}{10d}$	Max. rate of consumption for type II $\alpha(n)$ (Hall et al. 2007)
$\tilde{k}$	0.6×10^4	–	Half saturation constant for type II $\alpha(n)$ (Hall et al. 2007)
ρ	1	–	Relative feeding rate of infected individuals
f	0.75	$0 - 1$	Relative fecundity of infected individuals
χ	0.4×10^{-2}	–	Births per consumed resource (Duffy et al. 2005)
d_x	0.05	$0.02 - 0.1$	Host mortality $\approx$ per lifetime (per day) (Hall et al. 2006)
$\tilde{m}$	0.03	$0 - 0.5$	Fish predation rate (individuals per day) (Hall et al. 2006)
$\tilde{C}$	0.1	≤ 0.1	Consumption rate (type I $\alpha(n)$) (liters per day per consumer)
$\tilde{C}_c$	500	$0 - 1{,}000$	Max. $C(n)$ (type II $\alpha(n)$) (Porter et al. 1982)
η	0.7	$0 - 1$	Spore consumption efficiency
$\tilde{\beta}$	–	≥ 0	Infection rate (fit to give $\leq$20 % prevalence) (Hall et al. 2006)
$\tilde{\beta}_c$	–	≥ 0	Per capita per spore infection rate
$\tilde{\nu}$	d_x	$\approx d_x$	Additional non-fish-related mortality for infected individuals
θ	3	$1 - 10+$	Fish selectivity (Duffy et al. 2005; Hall et al. 2006)
$\tilde{\mu}$	0.033	≥ 0	Loss rate of infectious spores (no. per liter) (Hall et al. 2006)
σ	6.4×10^4	$0 - 10^5$	Spores produced per dead infected individual (Hall et al. 2006)

Units are individuals per liter, and time is in days. The broad range for d is based on the broad range of algal densities observed in nature. Growth rate r based on a range of 1–4 doublings per day

Eqs. 1b and 1c gives a reduced model with direct disease transmission,

$$\frac{dn}{dt} = rn(1-n) - \alpha(n)(x+y)n \tag{B2a}$$

$$\frac{dx}{dt} = \alpha(n)(x+fy)n - (1+m)x - B(n)xy \tag{B2b}$$

$$\frac{dy}{dt} = B(n)xy - (1+m\theta+\nu)y, \tag{B2c}$$

where $B(n)$ is the direct transmission rate, i.e., the rate of new infections per infectious individual (Eq. 5).

With this simplification, the force of infection now depends on the current density of infectives, by assuming that spores are so short-lived that the current spore density is proportional to the current density of infectives. The reduced and general models have the same equilibria for n, x, and y, and all of the bifurcations mentioned in the main text occur in both the general and reduced models.

Table 2 Parameters of the scaled model (Eq. 1)

Parameter	Value	Description
r	40	Producer growth rate (per day) (Sorokin and Krauss 1958)
α	–	Type I consumption rate (per consumer per day) (Hall et al. 2007)
a	–	Maximum of type II consumption rate $\alpha(n)$
k	–	Half saturation constant for type II $\alpha(n)$ (Hall et al. 2007)
ρ	1	Relative feeding rate of infected individuals
f	0.75	Relative fecundity of infected individuals
m	0.6	Fish predation rate on susceptible *Daphnia* (Duffy et al. 2005)
β	–	Infection rate (per susceptible per spore) (Duffy et al. 2005)
ν	1	Additional mortality for infected individuals unrelated to fish depredation
θ	3	Fish selectivity for infected individuals (Duffy et al. 2005; Hall et al. 2006)
σ	–	Spore production rate (per infected)
ϕ	0.5	Slope parameter for n-dependent spore production rate $\sigma(n)$
μ	0.66	Loss rate of infectious spores (per liter) (Hall et al. 2006)

Appendix C: Parameter values

Parameter values and ranges were determined based upon their biological interpretations, using published values of those quantities when available. Other values come from previously published models of *Daphnia* parasitism or algae consumption. Within biologically plausible parameter ranges, certain parameter values were further specified in order to yield dynamics consistent with field and laboratory observations or produce specific dynamic behaviors.

Algal growth and consumptions rates are based on the wide range of natural variability in green algae and their interactions with *Daphnia*. Intrinsic growth rate $\tilde{r}$ is based on 1–4 doublings day^{-1} for green algae (e.g., Sorokin and Krauss 1958) and maximum algal densities are based on naturally occurring levels during typical algal blooms.

Daphnia feeding (or filtering) rates were based on previously published population growth rates and observed feeding rates (Hall et al. 2007; Duffy et al. 2005; Porter et al. 1982, for example), though such rates in reality likely depend on other factors including temperature and food quality and thus are only loosely defined here. Under the units of milligrams dry weight per liter (as in Hall et al. 2007), we have maximum consumption rates $a \approx$ 1–2 orders of magnitude smaller than $N < K$, with k roughly of the same order of magnitude as K, though slightly smaller. Based on Duffy et al. (2005) where the maximum birth rate was 0.4 day^{-1} (with generation times of 1–3 weeks), we can assume that the maximum birth rate χa is equal to $b_{\max} = 0.4$ day^{-1} from Duffy et al. (2005), which implies (by $a \approx 10^2$ above) that $\chi = 0.4 \times 10^{-2}$.

Disease parameters given in Table 1 yield an $\mathcal{R}_{0,\mathrm{dis}}$ only slightly larger than 1 (though simulation suggests that this does not guarantee disease persistence in the presence of host–resource cycles). Thus, the spore-based infection rate was allowed to be somewhat flexible in order to attain prevalence levels consistent with those observed in naturally occurring *M. bicuspidata* epizootics.

The maximum per consumer filtering rate (liters per day) for *Daphnia magna* is taken from Fig. 1 of Porter et al. (1982), which suggests nearly 4 mL h^{-}1. Converting to the proper units and rounding yields approximately 0.1 L day$^{-1} = \frac{\tilde{C}_c}{\tilde{k}}$. With the above, we compute $\tilde{C}_c$ as $0.1k$.

To estimate plausible values of ϕ, we rely on the data in Fig. 1f of Hall et al. (2009a). The best fit line to those data gives $\sigma(1)/\sigma(0) = (1 + \phi n) \approx 0.03/0.02$, a quantity independent of σ_0. To use this to estimate ϕ, we must first know what weight corresponds to the algal carrying capacity (i.e., what n corresponds to 1 mg C/L?). Assuming that 1 mg C/L corresponds to the carrying capacity $n = 1$—a conservative (low) estimate—these data imply $\phi \approx 0.5$. If 1 mg C/L corresponds to some density below carrying capacity, then $\phi = 0.5/n > 0.5$. Thus, if carrying capacity corresponds to W (milligrams C per liter), then $\phi = W \cdot 0.5$. To avoid extrapolating beyond the available data, larger values of W may require a saturating or other functional form of $\sigma(n)$. In the text, we assume the conservative estimate of $\phi = 0.5$.

Appendix D: Consumer–resource models with slow disease dynamics

Disease can reduce consumer fecundity, increase consumer mortality, or both. How does this affect the consumer–resource dynamics? How do those changes affect disease dynamics? How is bistability maintained between cycling and steady-state dynamics in the presence of disease? To answer these questions, we consider a limiting case of model B2 with constant $B(n) = B$.

Assuming $x + y > 0$, we transform Eq. B2 to be in terms of resource density n, total consumers $p = x + y$, and fraction of infected consumers $i = y/(x + y)$. This is done by substituting $f = 1 - g \in (0, 1)$, $x = ip$ and $y = (1 - i)p$ into $dp/dt = dx/dt + dy/dt$ and $di/dt = (dy/dt)/p - i(dp/dt)/p$. Defining $R = B/(1 + \nu)$, this yields

$$\frac{dn}{dt} = \left(\frac{r}{\alpha(n)}(1 - n) - p\right)\alpha(n)n \tag{D1a}$$

$$\frac{dp}{dt} = \left(\alpha(n)n - \frac{1 + \nu i}{1 - gi}\right)(1 - gi)p \tag{D1b}$$

$$\frac{di}{dt} = \left(Rp(1 - i) - 1 - \frac{d\ln(p)}{dt}\frac{1}{1 + \nu}\right)(1 + \nu)i. \tag{D1c}$$

Here, the equations are factored to clarify their nullclines, and without loss of generality, we have assumed no predation on consumers ($m = 0$). (Compare Eq. D1 to Hilker and Schmitz (2008) for a similar model with frequency-dependent disease transmission and no bistability).

Assuming that the long-term disease dynamics (under Eq. D1) occur slowly relative to the consumer–resource dynamics, the n-p dynamics approach a quasi-asymptotic state (e.g., either steady-state or cycling dynamics) as i slowly changes. We can understand these quasi-asymptotic consumer–resource dynamics as follows:

Assuming constant $i \in (0, 1)$, the dynamics of Eqs. D1a and D1b can be understood from the n and p nullclines:

$$\frac{1}{n}\frac{dn}{dt} = 0 \quad \Rightarrow \quad p = \frac{r}{\alpha(n)}(1 - n) \tag{D2a}$$

$$\frac{1}{p}\frac{dp}{dt} = 0 \quad \Rightarrow \quad G(i) = \alpha(n)n. \tag{D2b}$$

where $G(i) = \frac{1+\nu i}{1-gi}$ is the fractional increase in the per-consumer mortality rate divided by the decrease in fecundity. Figure 6 shows an example of these nullclines using a type II functional response.

The p-nullcline (Eq. D2b) for fixed i is a vertical line at the equilibrium value of $n = n_{\text{eq}}$. The coexistence equilibrium occurs where these two nullclines intersect and is stable when (1) the per-capita feeding rate $\alpha(n)n$ is increasing at n_{eq} and (2) the n-nullcline (Eq. D2a) is decreasing at n_{eq}. Cycling dynamics occur if the n-nullcline is increasing at n_{eq} (where the coexistence equilibrium is unstable).

Prevalence i only affects the p-nullcline (Eq. D2a). Differentiating $\alpha(n)n = G(i)$ with respect to i, it follows that n_* typically *increases* as disease prevalence i increases since

$$\text{sign}\left(\frac{dn_*}{di}\right) = \text{sign}\left(\frac{d}{dn}(A(n_*)n_*)\right)\text{sign}\left(\frac{d}{di}G(i)\right). \tag{D3}$$

Consequently, a slow increase in disease prevalence should stabilize the system by increasing n_{eq} as shown in Fig. 6.

Why bistability?

Having described the consumer–resource dynamics under fixed i, we can clarify how density-dependent disease transmission leads to bistability by simplifying the disease (Eq. D1c). This can be done (albeit crudely) by considering the criterion for disease to invade the disease-free cycle LC_1 (see the next section for details):

$$R\overline{p_0} > 1. \tag{D4}$$

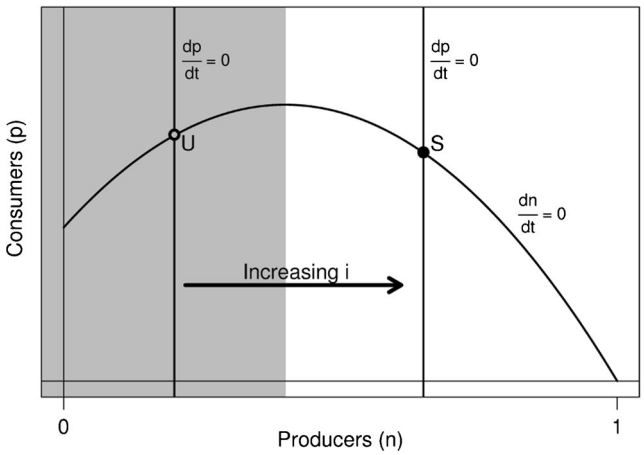

Fig. 6 Nullclines for the Rosenzweig–MacArthur model (type II $\alpha(n)$) illustrating the consequence of reduced fecundity and/or increased mortality among consumers. Assuming a fixed fraction (i) of the population are diseased, increasing i shifts the p-nullcline to the right, the direction of increasing stability. Changing i has no effect on the n-nullcline. The coexistence equilibrium is unstable where the n-nullcline is increasing (*shaded gray*, here the populations cycle) and is stable where the n-nullcline is decreasing. This is generally the case for any monotone increasing feeding rate $\alpha(n)n$ under Eqs. D1a and D1b

Here, $\overline{p_0}$ is the mean consumer density over the disease-free cycle. Note the similarity to the condition $\mathcal{R}_{0d} > 1$ necessary for invasion of the disease-free steady state EQ_1.

Based upon this observation, we approximate Eq. D1c by taking the "slow disease" limit of Eq. D1 which relies on the mean resource density $\overline{p_i}$ over the attracting cycle or equilibrium point determined by Eqs. D1a and D1b with fixed i.

Doing so yields the approximation

$$\frac{di}{dt} = i\,(\overline{p_i}\cdot(1-i) - 1/R)\,R. \tag{D5}$$

Computing $\overline{p_i}$ over a range of (fixed) i values, Fig. 7 shows how a disease-induced mortality and reduced fecundity can each increase mean consumer density during cycling regimes, when consumer–resource dynamics are fast relative to changes in i. This "hydra effect" (Abrams 2009) appears to be what allows for bistability when disease transmission is density-dependent. Positive feedback between p and i means that perturbing either a cycling system with little or no disease could sufficiently increase consumer density and push the system above threshold, allowing persistence of disease at steady state.

More precisely, Fig. 8 shows the $\overline{p_i}$ curve shown in Fig. 7 which shapes the dynamics of Eq. D5 for differing values of R. Stability is determined by where i is increasing ($\overline{p_i}(1-i) > 1/R$) and decreasing ($\overline{p_i}(1-i) < 1/R$), and the small peak in Fig. 8 is approximately where the Hopf bifurcation occurs in the consumer–resource model (Eqs. D1a and D1b). As in Fig. 7, equilibria to the left of this peak correspond to cycles under models Eqs. D1a and D1c and those to the right correspond to the endemic disease steady state EQ_2.

Figure 8 accounts for four of the five qualitatively different cases described for models Eqs. 1 and B2 in the text. Though not shown, if the "Hopf peak" was to surpass the critical value of $\overline{p_0}$ (the triangle in Fig. 8), then any values of $1/R$ between the peak's maximum value and $\overline{p_0}$ would yield bistability between disease-free cycles LC_1 and the endemic disease steady state EQ_2 as in region ④ of Fig. 4.

Criteria for invasion of disease-free limit cycles

Equation D1c is equivalent to

$$\frac{d(\ln i)}{dt} = (1+\nu)(Rp(1-i)-1) - \frac{d(\ln p)}{dt}. \tag{D6}$$

A criterion for the local stability of the disease-free limit cycle LC_1 (period T) can be obtained by considering the average rate of increase in i over that disease-free limit cycle assuming an arbitrarily small $i(0) > 0$. Define the instantaneous growth rate on LC_1 as

$$\lambda_i(t) \equiv (1+\nu)(Rp(1-i)-1) - \frac{d(\ln p)}{dt}. \tag{D7}$$

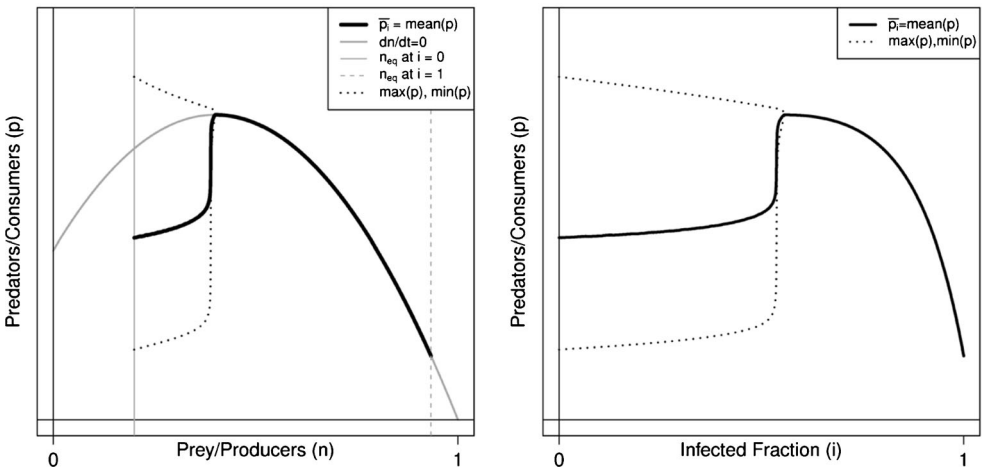

Fig. 7 Nullclines for the Rosenzweig–MacArthur model (type II $\alpha(n)$) illustrating how the "hydra effect" (Abrams 2009) in this model allows disease to paradoxically increase the mean resource density during cycling dynamics. The mean and amplitude of the consumer population are shown as the p-nullcline (*vertical line*) moves right as the fixed disease fraction (i) is increased from $i = 0$ to $i = 1$. Also shown is the mean $\overline{p_i}$ as a function of i. See Fig. 6 for other details

The average growth rate over LC_1 is therefore given by

$$\Lambda_T \equiv \frac{1}{T}\int_0^T \lambda_i(t)dt. \tag{D8}$$

thus, LC_1 is locally stable if $\Lambda_T < 0$ and disease invades if $\Lambda_T > 0$.

Combining the above equations yields

$$\Lambda_T = \frac{1}{T}\int_{0^T}(1+\nu)(Rp(1-i)dt - \frac{1}{T}\int_{0^T}\frac{d(\ln p)}{dt}dt \tag{D9}$$

$$= (R\overline{s}-1)(1+\nu) - \frac{1}{T}(\ln p(T) - \ln p(0)) \tag{D9}$$

where $\overline{s} \equiv \frac{1}{T}\int_0^T p(t)(1-i(t))dt$. On the limit cycle $p(T) = p(0)$ and $\overline{s} = \overline{s_0}$ where s_0 is the mean susceptible population size over the disease-free cycle. These two facts together with Eq. D9 yield the LC_1 stability criterion

$$R\overline{s_0} < 1. \tag{D10}$$

Note that in cases of bistability, sufficiently high initial levels of disease can push the system beyond the basin of attraction for disease-free cycle LC_1 and result in disease invasion despite $R\overline{s_0} < 1$ (Fig. 9).

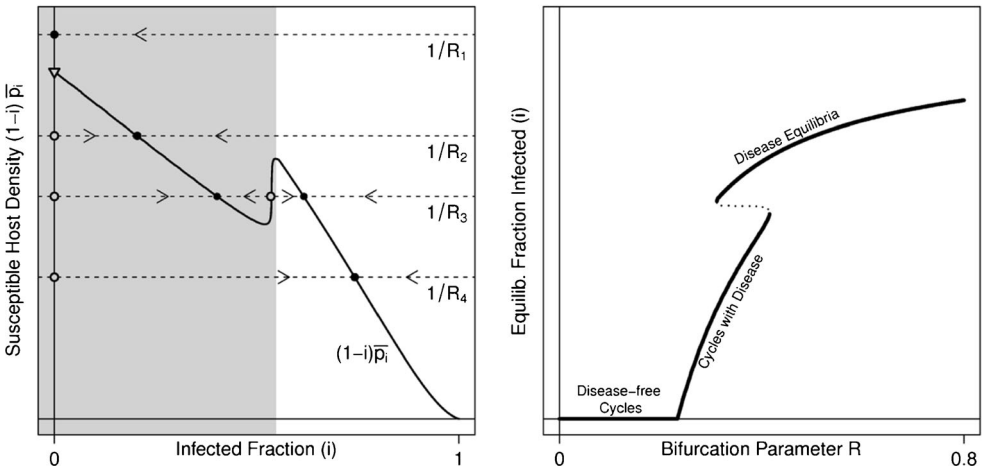

Fig. 8 Example dynamics of Eq. D5 for multiple values of parameter R. Equilibria in the region that is *shaded light gray* correspond to cycles under Eq. D1. Note $i > 0$ requires $R\overline{p_0} < 1$ (triangle at $i = 0$). In terms of the dynamics of models Eqs. D1 and B2, these equilibria correspond to dynamic states where only the disease-free cycle LC_1 is stable (R_1), only the disease cycle LC_2 is stable (R_2), both LC_2 and the endemic disease steady state EQ_2 are bistable (R_3), and only EQ_2 is stable (R_4). These correspond to the dynamics dominating regions ⑤, ②, ③, and ① in Fig. 4, respectively

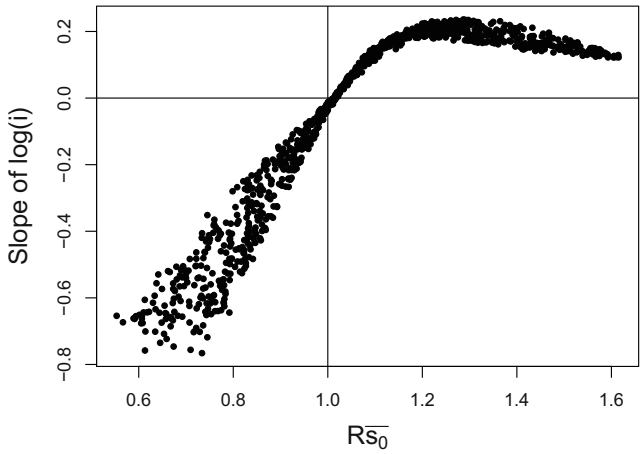

Fig. 9 Simulation showing the performance of the disease invasion criterion for the disease-free cycle LC_1 under constant–rates model (Eq. 1) with fast spore dynamics. Parameter values were sampled from uniform distributions with $\beta \in (5, 11)$, $f \in (0, 1)$, and $\nu \in (0, 3)$. Disease invasion is shown by the slope of the best-fit line to $\log(i(t))$ over 15 time units, with positive slope indicating disease invasion. The quantity $\bar{R}s_0$ is as described in the text. Parameters used: $r = 40$, $\alpha = 9$, $k = 0.6$, $m = 0$, $\mu = 1900$, and $\sigma = 90$

References

Abrams PA (2009) When does greater mortality increase population size? The long history and diverse mechanisms underlying the hydra effect. Ecol Lett 12:462–474

Anderson RM, May RM (1981) The population dynamics of microparasites and their invertebrate hosts. Phil Trans Roy Soc Lond B Biol Sci 291:451–524

Anderson RM, May RM (1991) Infectious diseases of humans: dynamics and control. Oxford University Press, Oxford

Armstrong RA, McGehee R (1980) Competitive exclusion. Am Nat 115:151–170

Bedhomme S, Agnew P, Sidobre C, Michalakis Y (2004) Virulence reaction norms across a food gradient. Proc Roy Soc Lond B Biol Sci 271:739–744

Bittner K, Rothhaupt K-O, Ebert D (2002) Ecological Interactions of the microparasite *Caullerya mesnili* and its host *Daphnia galeata*. Limnol Oceanogr 47:300–305

Cáceres CE, Knight CJ, Hall SR (2009) Predatorspreaders: predation can enhance parasite success in a planktonic hostparasite system. Ecology 90:2850–2858s

Cintrón-Arias A, Castillo-Chávez C, Bettencourt LMA, Lloyd AL, Banks H (2009) The estimation of the effective reproductive number from disease outbreak data. Math Biosci Eng 6:261–282

D'Amico V, Elkinton JS, Dwyer G, Willis RB, Montgomery ME (1998) Foliage damage does not affect within-season transmission of an insect virus. Ecology 79:1104–1110

de Roode JC, Yates AJ, Altizer S (2008) Virulence-transmission trade-offs and population divergence in virulence in a naturally occurring butterfly parasite. Proc Natl Acad Sci 105:7489–7494

Duffy M, Hall S (2008) Selective predation and rapid evolution can jointly dampen effects of virulent parasites on *Daphnia* populations. Am Nat 171:499–510

Duffy MA, Hall SR, Tessier AJ, Huebner M (2005) Selective predators and their parasitized prey: are epidemics in zooplankton under top-down control? Limnol Oceanogr 50:412–420

Duffy MA, Housley JM, Penczykowski RM, Cáceres CE, Hall SR (2011) Unhealthy herds: indirect effects of predators enhance two drivers of disease spread. Funct Ecol 25:945–953

Dwyer G, Dushoff J, Yee SH (2004) The combined effects of pathogens and predators on insect outbreaks. Nature 430:341–345

Dwyer G, Firestone J, Stevens TE (2005) Should models of disease dynamics in herbivorous insects include the effects of variability in host-plant foliage quality? Am Nat 165:16–31

Ebert D (2005) Ecology, epidemiology, and evolution of parasitism in *Daphnia*. National Library of Medicine (US), National Center for Biotechnology Information, Bethesda, MD. http://www.ncbi.nlm.nih.gov/entrez/query.fcgi?db=Books. Accessed 8 Feb 2008

Ebert D, Weisser WW (1997) Optimal killing for obligate killers: the evolution of life histories and virulence of semelparous parasites. Proc Roy Soc Lond B Biol Sci 264:985–991

Ebert D, Carius HJ, Little T, Decaestecker E (2004) The evolution of virulence when parasites cause host castration and gigantism. Am Nat 164:S19–S32

Ebert D, Zschokke-Rohringer CD, Carius HJ (2000) Dose effects and density-dependent regulation of two microparasites of *Daphnia magna*. Oecologia 122:200–209

Greenman J, Hudson P (1997) Infected coexistence instability with and without density-dependent regulation. J Theor Biol 185:345–356

Grover JP (1997) Resource competition. In: Population and community biology, vol 19. Chapman & Hall, London

Gubbins SC, Gilligan A, Kleczkowski A (2000) Population dynamics of plantparasite interactions: thresholds for invasion. J Theor Biol 57:219–233

Guckenheimer J, Myers M (1996) Computing Hopf bifurcations. II: three examples from neurophysiology. SIAM J Sci Comput 17:1275–1301

Guckenheimer J, Myers M, Sturmfels B (1997) Computing Hopf bifurcations I. SIAM J Numer Anal 34:1–21

Hall S, Duffy M, Cáceres C (2005) Selective predation and productivity jointly drive complex behavior in host-parasite systems. Am Nat 165:70–81

Hall SR, Tessier AJ, Duffy MA, Huebner M, Cáceres CE (2006) Warmer does not have to mean sicker: temperature and predators can jointly drive timing of epidemics. Ecology 87:1684–1695

Hall SR, Sivars-Becker L, Becker C, Duffy MA, Tessier AJ, Cáceres CE (2007) Eating yourself sick: transmission of disease as a function of foraging ecology. Ecol Lett 10:207–218

Hall S, Simonis J, Nisbet R, Tessier A, Cáceres C (2009a) Resource ecology of virulence in a planktonic host-parasite system: an explanation using dynamic energy budgets. Am Nat 174:149–162

Hall SR, Becker CR, Simonis JL, Duffy MA, Tessier AJ, Cáceres CE (2009b) Friendly competition: evidence for a dilution effect among competitors in a planktonic host-parasite system. Ecol 90:791–801

Hall SR, Knight CJ, Becker CR, Duffy MA, Tessier AJ, Cáceres CE (2009c) Quality matters: resource quality for hosts and the timing of epidemics. Ecol Lett 12:118–128

Hall SR, Smyth R, Becker CR, Duffy MA, Knight CJ, MacIntyre S, Tessier AJ, Cáceres CE (2010) Why are *Daphnia* in some lakes sicker? Disease ecology, habitat structure, and the plankton. BioScience 60:363–375

Hatcher MJ, Dick JTA, Dunn AM (2006) How parasites affect interactions between competitors and predators. Ecol Lett 9:1253–1271

Hethcote H (1973) Asymptotic behavior in a deterministic epidemic model. Bull Math Biol 35:607–614

Hethcote H, Levin S (1989) Periodicity in epidemiological models. In: Gross L, Hallam T, Levin S (eds) Applied mathematical ecology, vol 18. Springer, New York, pp 193–211

Hethcote HW, Stech HW, Driessche PVD (1981) Nonlinear oscillations in epidemic models. SIAM J Appl Math 40:1–9

Hilker FM, Schmitz K (2008) Disease-induced stabilization of predator-prey oscillations. J Theor Biol 255:299–306

Hilker FM, Langlais M, Malchow H (2009) The Allee effect and infectious diseases: extinction, multistability, and the (dis-)appearance of oscillations. Am Nat 173:72–88

Holmes EE (1997) Basic epidemiological concepts in a spatial context. In: Tilman D, Kareiva PM (eds) Spatial ecology: the role of space in population dynamics and interspecific interactions. Princeton University Press, Princeton, pp 111–136

Holt RD, Roy M (2007) Predation can increase the prevalence of infectious disease. Am Nat 169:690–699

Holt RD, Dobson AP, Begon M, Bowers RG, Schauber EM (2003) Parasite establishment in host communities. Ecol Lett 6:837–842

Hunter MD, Schultz JC (1993) Induced plant defenses breached? Phytochemical induction protects an herbivore from disease. Oecologia 94:195–203. doi:10.1007/BF00.341317

Hurtado PJ (2012) Infectious disease ecology: immune-pathogen dynamics, and how trophic interactions drive prey-predator-disease dynamics. PhD thesis. Cornell University

Jensen CX, Ginzburg LR (2005) Paradoxes or theoretical failures? The jury is still out. Ecol Model 188:3–14

Johnson PTJ, Chase JM, Dosch KL, Hartson RB, Gross JA, Larson DJ, Sutherland DR, Carpenter SR (2007) Aquatic eutrophication promotes pathogenic infection in amphibians. Proc Natl Acad Sci 104:15781–15786

Keating S, Schultz J, Yendol W (1990) The effect of diet on gypsy moth (*Lymantria dispar*) larval midgut pH, and its relationship with larval susceptibility to a baculovirus. J Invertebr Pathol 56:317–326

Keeling MJ, Rohani P (2008) Modeling infectious diseases in humans and animals. Princeton University Press, Princeton

Keesing F, Holt RD, Ostfeld RS (2006) Effects of species diversity on disease risk. Ecol Lett 9:485–498

Kirk KL (1998) Enrichment can stabilize population dynamics: autotoxins and density dependence. Ecology 79:2456–2462

Liu W-m, Levin SA, Iwasa Y (1986) Influence of nonlinear incidence rates upon the behavior of SIRS epidemiological models. J Math Biol 23:187–204

London WP, Yorke JA (1973) Recurrent outbreaks of measles, chickenpox and mumps. Am J Epidemiol 98:453–468

Matsuda H, Abrams PA (2004) Effects of predator-prey interactions and adaptive change on sustainable yield. Can J Fish Aquat Sci 61:175–184

McCauley E, Murdoch WW (1990) Predatorprey dynamics in environments rich and poor in nutrients. Nature 343:455–457

McCauley E, Nisbet RM, Murdoch WW, de Roos AM, Gurney WSC (1999) Large-amplitude cycles of *Daphnia* and its algal prey in enriched environments. Nature 402:653–656

Murdoch WW, Briggs CJ, Nisbet RM (2003) Consumer-resource dynamics. Monographs in population biology, vol 36. Princeton University Press, Princeton

Norman R, Bowers R, Begon M, Hudson P (1999) Persistence of tick-borne virus in the presence of multiple host species: tick reservoirs and parasite mediated competition. J Theor Biol 200:111–118

Ostfeld RS, Holt RD (2004) Are predators good for your health? Evaluating evidence for top-down regulation of zoonotic disease reservoirs. Front Ecol Environ 2:13–20

Ostfeld RS, Keesing F (2000) The function of biodiversity in the ecology of vector-borne zoonotic diseases. Can J Zool 78:2061–2078

Packer C, Holt RD, Hudson PJ, Lafferty KD, Dobson AP (2003) Keeping the herds healthy and alert: implications of predator control for infectious disease. Ecol Lett 6:797–802

Porter KG, Gerritsen J, Orcutt J, John D (1982) The effect of food concentration on swimming patterns, feeding behavior, ingestion, assimilation, and respiration by *Daphnia*. Limnol Oceanogr 27:935–949

Pulkkinen K, Ebert D (2004) Host starvation decreases parasite load and mean host size in experimental populations. Ecology 85:823–833

Regoes RR, Ebert D, Bonhoeffer S (2002) Dosedependent infection rates of parasites produce the Allee effect in epidemiology. Proc Roy Soc Lond B Biol Sci 269:271–279

Rosenzweig ML (1971) Paradox of enrichment: destabilization of exploitation ecosystems in ecological time. Science 171:385–387

Ryder JJ, Hathway J, Knell RJ (2007) Constraints on parasite fecundity and transmission in an insect-STD system. Oikos 116:578–584

Scheffer M, Rinaldi S, Kuznetsov YA, van Nes EH (1997) Seasonal dynamics of *Daphnia* and algae explained as a periodically forced predator-prey system. Oikos 80:519–532

Scheffer M, Rinaldi S, Kuznetsov YA (2000) Effects of fish on plankton dynamics: a theoretical analysis. Can J Fish Aquat Sci 57:1208–1219

Sieber M, Hilker F (2011) The hydra effect in predatorprey models. J Math Biol Online:1–20

Sorokin C, Krauss RW (1958) The Effects of light intensity on the growth rates of green algae. Plant Physiol 33:109–113

Tessier AJ, Woodruff P (2002) Cryptic trophic cascade along a gradient of lake size. Ecol 83:1263–1270

Tseng M (2004) Sexspecific response of a mosquito to parasites and crowding. Proc Roy Soc Lond B Biol Sci 271:S186–S188

Tseng M (2006) Interactions between the parasite's previous and current environment mediate the outcome of parasite infection. Am Nat 168:565–571